Using local gyrokinetic codes to study global ITG modes in tokamaks

P. A. Abdoul[1], D. Dickinson[1], C. M. Roach[2] and H. R. Wilson[1]

[1] *York Plasma Institute, Physics Department, University of York, YO10 5DQ, York, UK*

[2] *EURATOM/CCFE Fusion Association, Culham Science Center, Abingdon, OX14 3DB, UK*

Introduction

Local gyrokinetic codes assume that for high toroidal mode number, $n >> 1$, the local eigenvalue $\Omega_0(x,p)$ matches a unique global eigenvalue Ω for a particular choice of radius, x and ballooning angle p. But this is only true for specific parameter sets where $\Omega_0(x,p)$ has a stationary point for which a so-called isolated mode is observed [1]. It typically peaks at the outboard mid plane, $\theta = 0$, and has a growth rate equal to the maximum, $\gamma_{max} = Max(\gamma_0(x,p))$. In general, the equilibrium profile variations reduces the global growth rate $\gamma < \gamma_{max}$ and shifts the mode away from the outboard mid plane. This introduces a discrepancy between the local and global calculations, which might have an important consequence, especially where the linear local growth rate is used to predict the quasilinear heat and particle transport. In this work we develop a formalism to link local and global linear gyrokinetic calculations. We have used solutions from the local gyrokinetic code GS2 [3] and applied higher order ballooning theory [4] to reconstruct the global linear electrostatic ITG modes in the $s-\alpha$ equilibrium model.

The Model and the technique

In this work, for simplicity, we have employed the $s-\alpha$ equilibrium model, which assumes high aspect ratio and circular magnetic flux surfaces. We have limited ourselves to linear electrostatic ITG modes with adiabatic electrons. The model parameters, used throughout this work, are listed in table 1. We have scanned GS2 many times over a range of radial points, x, and ballooning angle, $-\pi \leq p \leq +\pi$. This can provide the local mode structure $\xi(x,\theta,p)$ and the complex mode frequency $\Omega_0(x,p)$. Here, $x = (r-r_0)/a$ measures the distance from some rational surface at $r = r_0$ and normalised to the minor radius a. The main equation that lies at the heart of this paper is the Fourier ballooning representation for the electrostatic potential, $\phi(x,\theta)$:

$$\phi(x,\theta) = \int_{-\infty}^{\infty} \xi(x,p,\theta)\exp(-inq_0\theta)\exp(-inq'x(\theta-p))A(p)dp, \quad (1)$$

where the amplitude envelope $A(p)$ can be obtained from higher order ballooning theory by firstly fitting a model to $\Omega_0(x,p)$ using Fourier and Taylor expansion techniques as follows:

$$\Omega_0(x,p) = \sum_{k=0}^{N_k}\sum_{m=0}^{2} a_k^{(m)} x^m cos(kp), \quad (2)$$

Table 1: The model parameters that have been used throughout this paper. Note that they have been evaluated at mid radius, where $x = \frac{r-r_0}{a} = 0$.

Parameter	$\hat{s}$	q_0	R/L_T	R/L_n	$k_y\rho_i$	ε	a	R	β	nq'	$\nu_{ii} \times \frac{R}{v_{ti}}$	$\frac{T_i}{T_e}$
Value	1.5	1.4	17.0	2.2	0.45	0.18	0.27m	1.50m	0.0	300	0.8	1.0

where we retain N_k Fourier modes. Imposing the eigenvalue constraint $\Omega = \Omega_0(x,p)$ and using equation 1 to transform x and x^2 we have:

$$x \longrightarrow \frac{-1}{inq'}\frac{1}{A(p)}\frac{dA(p)}{dp}$$
$$x^2 \longrightarrow \frac{-1}{n^2q'^2}\frac{1}{A(p)}\frac{dA^2(p)}{dp^2} \tag{3}$$

One can then rewrite equation 2 as the following differential equation for $A(p)$ and its eigenvalue Ω:

$$\left[\sum_{k=0}^{N_k} a_k^2 cos(kp)\right]\frac{d^2A(p)}{dp^2} - \left[inq'\sum_{k=0}^{N_k} a_k^1 cos(kp)\right]\frac{dA(p)}{dp} - \left[n^2q'^2\sum_{k=0}^{N_k} a_k^0 cos(kp)\right]A(p) = -\left[n^2q'^2\Omega\right]A(p) \tag{4}$$

Solution of this equation provides $A(p)$ which can be used, along with ξ to calculate the global mode structures, $\phi(x,\theta)$, from equation 1.

The radial η_i profile

We introduce a quadratic radial profile for the mode drive η_i, namely $\eta_i = 17.00 - 1500x^2$. For simplicity, we have assumed that all other equilibrium profiles are constant over the radial domain of interest. The numerical solutions of equation 4 shows that the global eigenvalue Ω converges to a constant value for $k \geq 6$. For this reason in our calculations we have used the number of Fourier modes, $N_k = 7$. As we expected, we have found that all the coefficients with $m = 1$ are zero. As we an see from figure 1, both real frequency ω_0 (a) and

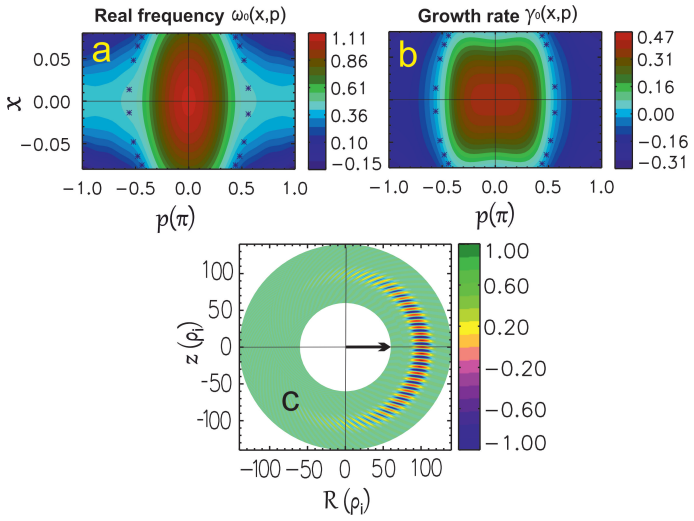

Figure 1: *The local real frequency $\omega_0(x,p)$ (a), growth rate $\gamma_0(x,p)$ (b) and the poloidal cross section for the reconstructed global mode structure, $\phi(x,\theta)$ (c).*

growth rate γ_0 (b) are stationary at $x = 0$, which leads to a highly unstable global mode, reconstructed using equation 1, known as the isolated mode [1] (figure 1-c). This mode peaks at the outboard mid-plane at $\theta = 0$ with growth rate, normalised to $\frac{v_{ti}}{R}$, $\gamma = 0.461$. Here v_{ti} is the ion thermal speed. When the toroidal mode number, $n >> 1$, this global growth rate matches the maximum value of local growth rate $\gamma_0(x,p)$, i.e $\gamma = \gamma_0(0,0) - (\sim (1/n))$. This is often assumed in local flux tube calculation. However it is true when the effect of other profile variations are not taken into account. Such a profile variation, as we see in the following section, introduces a discrepancy between the local and global growth rates.

Flow shear and profile variation effects

The effect of flow shear has been investigated through a Doppler shift in real frequency, $\Omega_0 \rightarrow \Omega_0 + n\Omega' x = (\omega_0 + n\Omega' x) + i\gamma_0$. Where $\Omega' = d\Omega_R/dx$, Ω_R is linear in x and represents the rotational angular frequency of the surfaces with respect to the rational surface at $x = 0$. The flow shear, Ω', removes the stationary point from Ω_0, modifying the isolated mode.

Depending on the sign of the flow shear, the reconstructed global mode shifts upward or downward with respect to the out board mid plane and reduces its growth rate, i.e $\gamma_{(\Omega' \neq 0)} < \gamma_{max}$. Furthermore, we introduce profile variation using a radially increasing q-profile, $q = 3.9(r/a)^{\hat{s}}$, with constant magnetic shear $\hat{s} = 1.5$. This breaks the poloidal symmetry of the the isolated mode about the out board mid plane and shifts it slightly downward with a slight reduction, $\approx 3\%$, in the growth rate. It also introduces an asymmetry, which is absent otherwise (see figure 2-a), into the growth rate spectrum with respect to the sign of the flow shear (see figure 2-b). As can be seen from figure 2-b, for a critical value of flow shear, nΩ′=-1.5, the growth rate reaches it is maximum value; the effect of the flow and q-profile variations cancel, and an isolated mode is observed.

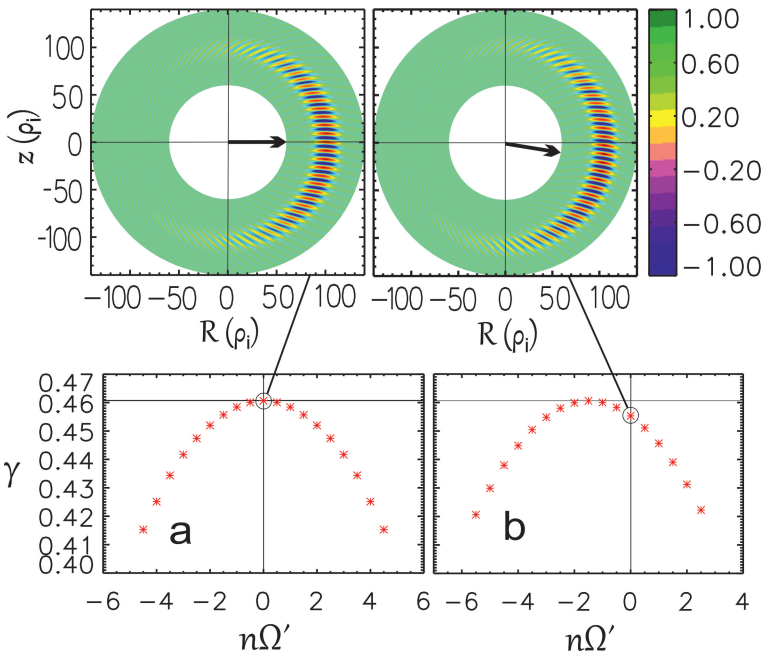

Figure 2: *The growth rate spectrum as a function of flow shear, $n\Omega'$, without (a) and with (b) profile variation effects. The contour plot for the reconstructed global mode structures for $n\Omega' = 0$ are also presented for each case.*

This finding, that we have obtained purely from solutions of the local gyrokinetic code GS2, has also been observed in global gyrokinetic simulations [2].

Conclusion

We have used solutions from a local gyrokinetic code, GS2, and combined it with higher order ballooning theory to reconstruct the global mode structures. A quadratic η_i profile yields an isolated mode with strong growth rate that peaks at $\theta = 0$. Including a radial q-profile variation breaks the poloidal symmetry of the isolated mode about $\theta = 0$ and reduces its growth rate. It also introduces an asymmetry to the growth rate spectrum with respect to the sign of flow shear. More generally we do not expect the global gyrokinetic codes to capture an isolated mode, except for a critical value of flow shear. In this work we have developed a powerful technique that enables us to compare the linear growth rate calculations between local and global simulations, for different radial profile variations. In our future work, investigating the effect of magnetic flux surface shaping together with taking realistic experimental tokamak geometries into consideration will be carried out.

Acknowledgment

The work is funded by the Ministry of Higher Education in Kurdistan region of Iraq and has also received funding from the European Union's Horizon 2020 research and innovation programme under grant agreement number 633053 and from the RCUK Energy Programme [grant number EP/I501045]. The views and opinions expressed herein do not necessarily reflect those of the European Commission. The simulations presented were carried out using supercomputing resources on HECToR (from the Plasma HEC Consortium EPSRC grant number EP/L000237/1). A part of this work was also carried out using the HELIOS supercomputer system at Computational Simulation Centre of International Fusion Energy Research Centre (IFERC-CSC), Aomori, Japan, under the Broader Approach collaboration between Euratom and Japan, implemented by Fusion for Energy and JAEA.

References

[1] D. Dickinson, et al. Physics of Plasmas **21** (2014) 010702
[2] P Hill, et al. Plasma Phys. Control. Fusion **54** (2012) 065011
[3] G. Rewoldt M. Kotschenreuther and W. M. Tang. Com. Phys. Communications, **88** (1995).
[4] J. B. Taylor, et al. Plasma Phys. Control. Fusion **38** (1996) 243-250